EasyChair Preprint

№ 9165

Design, Simulation and Analysis of a Matlab/Simulink Based Delay-and-Sum Beamforming Model for Ultrasound Imaging

Gilson Maekawa Kanashiro,
Michel Andrey Freitas de Souza Kohler,
Ednilson de Souza Contieri, Rojelio de Bairro,
Larissa Comar Neves, Thiago Mathias Oliveira,
Amauri Amorin Assef, Joaquim Miguel Maia and
Eduardo Tavares Costa

October 26, 2022

Design, simulation and analysis of a Matlab/Simulink based delay-and-sum beamforming model for ultrasound imaging

G.M. Kanashiro[1,2], M.A.F.S. Kohler[1], E.S. Contieri[1], R. Bairro[1], L.C. Neves[1], T.M. Oliveira[1], A.A. Assef[1,3], J.M. Maia[1,4] and E.T. Costa[5]

[1] Graduate Program in Electrical and Computer Engineering (CPGEI), Federal Univ. of Technology – Paraná (UTFPR), Curitiba, Brazil
[2] Federal Institute of Paraná (IFPR), Paranavaí, Brazil
[3] Academic Department of Electrical Engineering (DAELT), UTFPR, Curitiba, Brazil
[4] Biomedical Engineering Program (PPGEB) and Academic Department of Electronics Engineering (DAELN), UTFPR, Curitiba, Brazil
[5] DEEB-FEEC & CEB, University of Campinas (UNICAMP), Campinas, Brazil

Abstract— **In ultrasound research, an important subject is the quality of image assessment. Despite a myriad of technological solutions, qualitative and quantitative metrics are critical indicators to measure and compare the quality of ultrasound images. This paper presents a simulation of a model that implements step-by-step an image reconstruction based on delay-and-sum (DAS) method from the Matlab/Simulink environment. The general objective was to validate this model to compare the quality metrics of images against the computational one. Model results were validated using the Field II as gold reference, a program for simulating ultrasound transducer fields and ultrasound imaging using linear acoustics. The model implements DAS beamforming to process 65 scanlines generated by a 128-element transducer. For quantitative analysis, the following metrics have been used: contrast resolution (CR), contrast-to-noise (CNR), signal-to-noise ratio (SNR), normalized root mean square error (NRMSE), normalized residual sum of squares (NRSS), and full width at half maximum (FWHM). According to those metrics, the proposed model performance is strongly correlated comparatively to the reference, showing errors of 1.49 %, 1.29 %, 0.22 %, 2.45 %, 7.38 % for the CR, CNR, SNR, FWHM, and NRMSE, respectively. As indicated by metrics the Matlab/Simulink model images are similar to the computational ones.**

Keywords— **Ultrasound, delay-and-sum, B-mode image, quality indicators, image quantifiers.**

I. Introduction

Ultrasound (US) medical images are non-invasive, free of ionizing radiation, and relatively cost-effective compared with x-ray systems. For these reasons, US technology has become widely used in diagnosis medicine.

In US research, it is necessary to assess the quality of an image despite of a myriad of technological solutions. As these various solutions address image quality comparison problems, studies on qualitative and quantitative metrics are justified as critical indicators to measure and compare the quality of US images.

The objective of this work was to validate a simulated model by comparing its image quality metrics against the computational model. Simulated model results were validated using the Field II [1] as gold reference, a program for simulating ultrasound transducer fields and ultrasound imaging using linear acoustics.

First, a computational (Matlab/Field II) model implemented a step-by-step image reconstruction. Next, a simulated (Simulink) model do the same approach to be validated. Both implementations were based on delay-and-sum (DAS) method to reconstruct a US image [2], [3]. This technique is considered well-established. However, to improve the image quality and accuracy of medical diagnosis, the raw radio-frequency (RF) signal needs to be manipulate directly [4], customizing the simulation of signal processing in real-time. More than that, it is necessary to measure the quality of images generated.

The functional block diagram Fig. 1 shows a general overview of the computational and simulated models. Next, the diagram and the US image processing steps will be explained briefly.

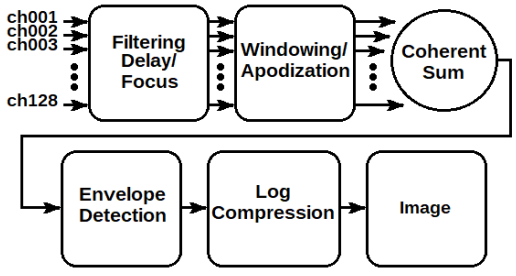

Fig. 1: Receive beamformer - functional steps to obtain DAS B-mode images

It illustrates the main steps of DAS beamforming sig-

nal processing for US images: filtering, delay/focalization, windowing/apodization, coherent summation, envelope detection, logarithmic compression, and image composition.

About that mentioned computational model, to simulate the transmission/reception, the aperture for emission/reception, the impulse response, and the excitation were configured by Field II functions.

Special attention was paid to the backscattered signal obtained by reception process. So with Matlab code and tools with Field II functions, it was implemented Hanning windowing focalization, filtering, coherent summation, envelope detection, logarithmic compression and image forming by scanlines juxtaposition.

Table 1: Transducer parameters and excitation data

Parameter	Values	Units
Linear array transducer	128	un
Active elements in the transducer	64	un
Transducer center frequency	3.2	MHz
Scanlines generated	65	un
Sampling frequency	40	MHz
Speed of sound (soft tissue)	1540	$m.s^{-1}$
Wavelength (λ)	481.25	μm
Width of element	481.25	μm
Height of element	5	mm
Kerf	8	μm
Fixed focal point (x,y,z)	[0,0,50]	mm
Elements in x-direction	1	un
Elements in y-direction	5	un
Targets simulated with phantom	20	un
Axial target separation	10	mm
Apodization	Hanning	-

II. Methods

Simulations have been done in Field II [1], a program for simulating ultrasound transducer fields and ultrasound imaging using linear acoustics, to reconstruct a 20-target axial image with focalization at 50 mm depth. For transmission, the parameters were set up considering a 128-element linear array transducer available in our laboratories. Table 1 shows usual units of measurement. The "un" symbol means quantities of units or elements.

A DAS model to generate the US image was built using Matlab/Simulink, whose quality was evaluated. There are two major tasks to reach the main goal of this work: the reconstruction of the B-mode image and the appliance of metrics to assess the image's quality.

A. B-mode image reconstruction

A 128-element transducer, with an aperture of 64 elements, has been used to receive scattered echoes (raw RF signal) to reconstruct US images. The received signals are processed using a low-pass filter (LP_Filter, Fig. 2) and delayers (Z^{-1}, Fig. 2) to provide a more precise and the correct focalization. The same approach described in [5] has been used to implement the LPF.

Next, a signal processing windowing technique, the apodization (Apod, Fig. 2) eliminates distortions caused by the lateral channels of the aperture. Here, a symmetric aperture was applied using the delay and apodization coefficients calculated by Field II.

The coherent summation, an adding operation of the 64 resulting signals $x(:,1)$ to $x(:,64)$ was executed recursively to generate the 65 scanlines (128 transducer's elements - 64 aperture's elements + 1). Fig. 2 illustrates these steps performed by 64 channels signal processing.

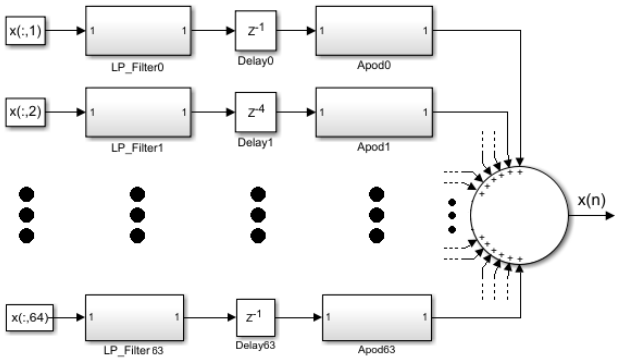

Fig. 2: Ultrasound DAS beamforming method. Block diagram illustrating the 64-channels of the first steps (acquisition, filtering, delay, apodization, and coherent summing)

The envelope detector will apply a Hilbert Transform (FIR Filter Hilbert Transformer, Fig. 3) to perform quadrature demodulation and determine an envelope curve ($E(n)$, Fig. 3) from an input RF signal ($x(n)$, Fig. 3). This detection corresponds to a tangent curve that involves each scanline $x(n)$.

As found in [6], envelope detection can be performed by modeling a Hilbert filter, using finite impulse response (FIR) techniques to obtain the phase $I(n)$ and quadrature $Q(n)$ components. A block diagram (Fig. 3) illustrates the concept behind these steps, whose details can be found in [7].

Usually, the dynamic range of the signal is restricted, as in [4] and [8], because of a limitation to viewing grayscale. The

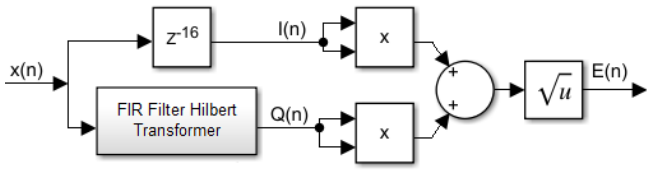

Fig. 3: Functional block diagram of envelope detector (quadrature demodulation)

dynamic range of human eyes can distinguish a 30 dB order. The dynamic range used in this work was restricted from -60 dB to 0 dB and the grayscale gradients from 0 (white) to 128 or 256 (black) with a so-called logarithmic compression. Additionally, this compression improves the contrast of the US image.

The rest of the process is related to conforming the generated image to the screen. A juxtapose operation is sufficient for the linear array transducer used to exhibit a B-mode image.

B. The B-mode image assessment

US B-mode images can generated following the steps described in the last section and illustrated by Fig. 1. For quantitative analysis, following metrics have been used: contrast resolution (CR), contrast-to-noise (CNR), signal-to-noise ratio (SNR), normalized root mean square error (NRMSE), normalized residual sum of squares (NRSS), and full width at half maximum (FWHM). Those metrics were evaluated after logarithmic compression to assess the overall image processing. Moreover, the region of interest (ROI) was defined at the target located at 50 mm and its neighborhood where applicable. Only the central scanline was considered for metrics dependent on scanlines to calculate the image quality metrics.

A straightforward notion about these quality image quantifiers is described in the following lines.

B1 Contrast metrics

Contrast is a measure of the ability to distinguish luminance between different regions of the displayed images [2]. Logarithmic compression, image memory, dynamic range, and contrast agents are variables that influence this parameter. In this work, CR (1) was employed as defined in [9], and CNR (2) as defined in [10]. These two contrast quantifiers were applied like [11] and [7] using equations 1 and 2:

$$CR = \left|\mu_{tgt} - \mu_{bck}\right|, \tag{1}$$

$$CNR = \frac{\left|\mu_{tgt} - \mu_{bck}\right|}{\sqrt{\sigma_{tgt}^2 + \sigma_{bck}^2}}, \tag{2}$$

where μ_{tgt} e μ_{bck} are mean intensities of target (tgt) and background (bck) regions, respectively. The σ_{tgt} and σ_{bck} are standard-deviations of the signal intensities in tgt and bck regions.

B2 Signal-to-noise ratio

The signal-to-noise ratio (SNR) compares the signal and the noise levels at a determined ROI. Its general goal is to quantify the image quality through speckle measurement [12]. Speckles are a kind of artifact (alteration) that accentuates the granular aspect, making the image resultant not correspond to the target's actual image.

A well-known approach to measuring SNR is through the mean intensity (μ_s) and the standard deviation (σ_s) of the signal [13], [14], defined as:

$$SNR = \frac{\mu_s}{\sigma_s} = \frac{\frac{1}{mn} \cdot \sum_{j=1}^{m} \sum_{i=1}^{n} E(i,j)}{\sqrt{\frac{1}{mn-1} \cdot \sum_{j=1}^{m} \sum_{i=1}^{n} \left(E(i,j) - \frac{1}{mn} \cdot \sum_{j=1}^{m} \sum_{i=1}^{n} E(i,j) \right)^2}} \tag{3}$$

where $E(i,j)$ is the intensities of signals, i and j are a row and a column within an ROI, respectively.

B3 Evaluating the goodness of fit

In regression analysis, it is common to measure the strength of the relationship between data. In our experiments, data are relative to numerical computation and simulated model one. The normalization data operation is to guarantee the same proportion.

In this work, the normalized residual sum of squares (NRSS) was used as a technique that quantifies the amount of error variance in the dataset. So, as residual summing, the nearer to zero is the NRSS metric, the best fit it is [15].

The normalized root mean square error (NRMSE) or normalized root mean square deviation (NRMSD) is the standard deviation of residuals (error prediction) and measures the average squared error between data. Although smaller NRMSE reflects greater accuracy, it is essential to remark that there is no best value for it [16]. The comparison of the computational and modeled system, the NRSS [17], and the NRMSE

[18] were employed with algorithms similar to [7],

$$NRSS = \frac{\sum_{k=0}^{M-1} |E(k) - ht(k)|^2}{\sum_{k=0}^{M-1} |ht(k)|^2} \tag{4}$$

$$NRMSE = 100 \cdot \sqrt{\frac{\sum_{k=0}^{M-1} |E(k) - ht(k)|^2}{\sum_{k=0}^{M-1} \left|ht(k) - \overline{ht}\right|^2}} \tag{5}$$

where ht and $\overline{ht}$ are the simulated envelope and the average value of it, respectively, $E(k)$ is the golden standard and M is the number of samples.

B4 Geometric distortion

The quantifier called full width at half maximum (FWHM) measures the geometric distortion. In this work, the FWHM reports the width between two points belonging to the central scanline curve, whose line intercepts half of its maximum value, or better said, at -6 dB from the maximum of the main lobe [8]. Fig. 4 shows the concept of FWHM. Two segment points are located at half amplitude $A/2$, in dB, x_1 and x_2, whose length is FWHM.

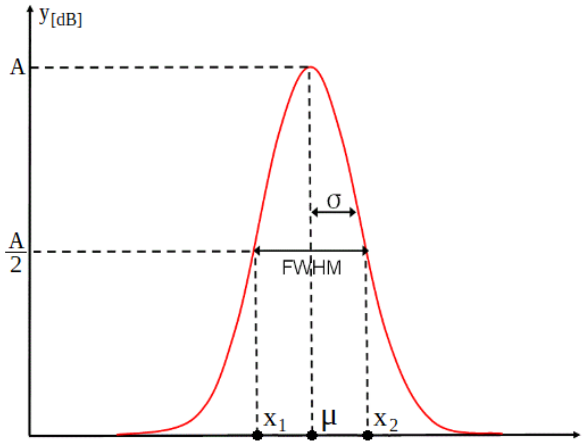

Fig. 4: Standard deviation σ and full width at half maximum $FWHM$

III. Results and Discussion

The proposed method (modeled system) was implemented to generate the image through all the steps illustrated in Fig. 1.

This work integrates image quality metrics found in different articles, each of them assessing some property of US image. Because of that, observations about this set of metrics were parted by subjects. CR and CNR are employed according to [9] and [10], respectively, and their application are according to [11] and [7]. SNR is widely applied, and the current approach is like [13] and [14]. The goodness of fit, NRSS and NRMSE was applied like [7]. Frequently, geometric distortion is considered. So FWHM was applied following [8] approach.

Considering the qualitative analysis, the envelope and the amplitude plot of the central scanline (of number 32) at the 50 mm target (Fig. 5a) was evaluated. Signals and their envelopes from the computational and modeled system show an excellent fit adjustment, as seen in Fig.5b, at the location pointed by an arrow in Fig. 5a.

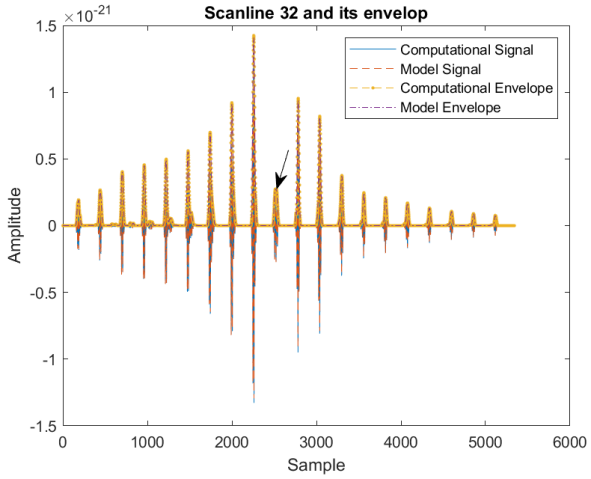

(a) The 20-targets scanline signal and its envelope

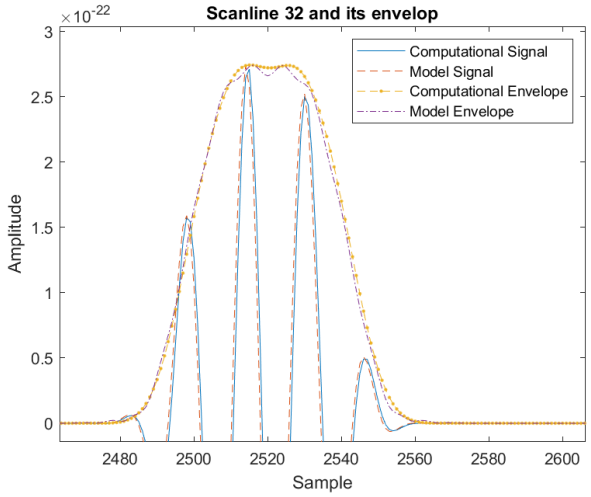

(b) Zoomed view of the signals indicated by the arrow

Fig. 5: **a** Scanline and envelope **b** Zoomed signal and envelope details of computational and modeled system showing similarity

Another approach is comparing both generated US images. Here, the similarity of both images is remarkable, as

shown in the resulting image of Fig. 6, where the accuracy of the model is quite evident even if considering the 20-targets. The squares with yellow (left) and blue (right) borders highlight the target and background areas, respectively. The target area and neighborhood were zoomed in for careful qualitative analysis. In Fig. 7, there is an arrow to indicate the slight difference related to the golden standard.

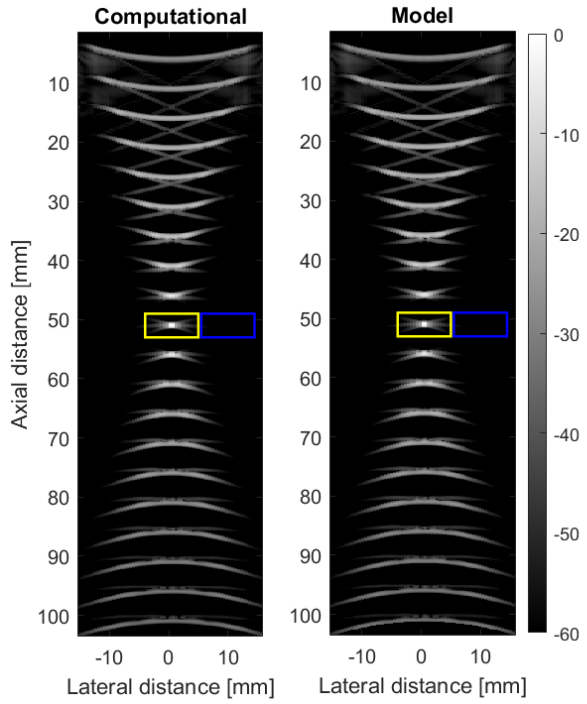

Fig. 6: Image qualitative evaluation. The model is similar to the computational one inside the corresponding rectangles

The proposed method results were compared to the computational Field II solution. After applying filtering in the raw signal, delays, apodization, and coherent summation, the envelope curve of the signal was generated.

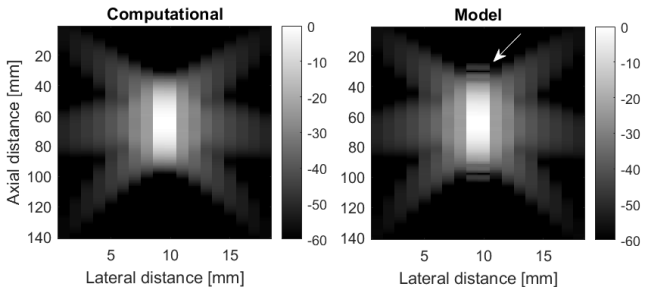

Fig. 7: Qualitative analysis of accuracy. Detail (arrow) of the model target showing slight difference

For the qualitative analysis, the goodness of fit was exhibited by Fig. 5a and 5b. This accuracy characteristic can be seen in Fig. 6, whose quality is detailed in a zoomed Fig. 7. For the quantitative analysis, relative to Table 2, it is noticeable that CR, CNR, SNR, and FWHM have very similar values between computational data and the model. The CR and CNR contrast metrics are better in the model as they are the greatest. The NRMSE shows a low value (less than 8%), which is considered an excellent approximation, and in particular, the near-zero NRSS refers to a good fit. Both computational and modeled systems show an excellent agreement.

Table 2 summarizes the results to be analyzed. The first column shows the image quality metrics. The second and third columns show values relative to the computational simulation and the modeled system from Matlab/Simulink. The last column shows the error percentage between the assessment percentual values of the systems. The two last lines show the goodness of fit metrics, calculated for both systems. Note that Table 2 groups apart NRMSE and NRSS because these metrics include both computational and modeled system parameters in their formulation.

Table 2: Image quality evaluation metrics

Metrics	Methods		
	Computational	Modeled	Error (%)
CR	10.01 dB	10.16 dB	1.49 %
CNR	0.77 dB	0.78 dB	1.29 %
SNR	-6.20	-6.19	0.22 %
FWHM	0.55 *mm*	0.56 *mm*	2.45 %
Goodness of fit metrics			Values
NRMSE (Computational versus Modeled)			7.38%
NRSS (Computational versus Modeled)			3.36×10^{-4}

IV. Conclusion

This work compared two simulations: a computational implemented with Field II add-on for Matlab and a modeled one made in Matlab/Simulink. A DAS beamforming model generates US scanlines and images in both systems. Some image quality metrics were adopted to evaluate the signals and images. For qualitative and quantitative assessment, the results of the modeled system were compared to the computational simulation (reference). Both computational and modeled systems show an excellent agreement.

This fact indicates that the modeling method in Matlab/Simulink could shorten the image quality assessment. Moreover, it was possible to model an entire DAS beamforming image with a minimum quality degradation of US images.

CONFLICT OF INTEREST

The authors declare that they have no conflict of interest.

ACKNOWLEDGEMENTS

The authors would like to thank the Brazilian Agencies Coordination for the Improvement of Higher Education Personnel (CAPES - Processo 001), National Council for Scientific and Technological Development (CNPq), Araucária Foundation, Financial Agency for Studies and Projects (FINEP), and Ministry of Health for the financial support.

REFERENCES

1. Jensen J A. FIELD: A Program for Simulating Ultrasound Systems in *10th Nordicbaltic Conference On Biomedical Imaging, Vol. 4, Supplement 1, Part 1:351–353*:351–353 1996.
2. Hedrick W R, Hykes D L, Starchman D E. *Ultrasound Physics and Instrumentation*. Missouri: Mosby Inc. 1995.
3. Thomenius K E. Evolution of ultrasound beamformers *IEEE Ultrasonics Symposium. Proceedings.* 1996;2:1615-1622.
4. Assef A A, Maia J M, Costa E T. Initial experiments of a 128-channel FPGA and PC-based ultrasound imaging system for teaching and research activities in *2016 38th Annual International Conference of the IEEE Engineering in Medicine and Biology Society (EMBC)*:5172-5175 2016.
5. Assef A A, Oliveira J, Scherbaty L, et al. *Modeling of a Simple and Efficient Cascaded FPGA-Based Digital Band-Pass FIR Filter for Raw Ultrasound Data*:501-505 . 2019.
6. Oppenheim A V. *Discrete-time signal processing* . 1999.
7. Assef A A, de Oliveira J, Maia J M, Costa E T. FPGA Implementation and Evaluation of an Approximate Hilbert Transform-Based Envelope Detector for Ultrasound Imaging Using the DSP Builder Development Tool in *2019 41st Annual International Conference of the IEEE Engineering in Medicine and Biology Society (EMBC)*:2813-2816 2019.
8. Da Silva Ruzyk M J, Martinez A C, Assef A A, De Oliveira L R, Maia J M, Costa E T. Comparison of three simulation methods for RF ultrasound signal envelope detection in *2021 IEEE UFFC Latin America Ultrasonics Symposium (LAUS)*:1-4 2021.
9. Xu M, Yang X, Ding M, Yuchi M. Spatio-temporally smoothed coherence factor for ultrasound imaging [Correspondence] *IEEE Transactions on Ultrasonics, Ferroelectrics, and Frequency Control.* 2014;61:182-190.
10. Rindal O M H, Åsen J P, Holm S, Austeng A. Understanding contrast improvements from capon beamforming in *2014 IEEE International Ultrasonics Symposium*:1694-1697 2014.
11. Zimbico A J. *Bayesian-based beamformer with wiener post-filter for adaptative processing of ultrasond image using coherent plane wave compounding*. PhD thesisUniversidade Tecnológica Federal do Paraná (UTFPR)Curitiba 2019. PhD Thesis (CPGEI).
12. Schiefler N, Maia J, Schneider F, Zimbico A, Assef A, Costa E. Generation and Analysis of Ultrasound Images Using Plane Wave and Sparse Arrays Techniques *Sensors.* 2018;18:3660.
13. Omari E A, Varghese T. Signal to noise ratio comparisons for ultrasound attenuation slope estimation algorithms. *Med. Phys.*. 2014;41:032902.
14. Tasnim T, Shuvo Md. M H, Hasan S. Study of speckle noise reduction from ultrasound B-mode images using different filtering techniques in *2017 4th International Conference on Advances in Electrical Engineering (ICAEE)*:229-234 2017.
15. Draper N R, Smith H. *Applied Regression Analysis* . 1998.
16. Salkind N J. *Encyclopedia of Research Design*. No. v. 1Sage 2010.
17. Zhou H, Zheng Y F. An efficient quadrature demodulator for medical ultrasound imaging. *Frontiers of Information Technology & Eletronic.* ;16.
18. Levesque P, Sawan M. Real-Time Hand-Held Ultrasound Medical-Imaging Device Based on a New Digital Quadrature Demodulation Processor *IEEE Transactions on Ultrasonics, Ferroelectrics, and Frequency Control.* 2009;56:1654-1665.

Corresponding author:

Author: Gilson Maekawa Kanashiro
Institute: Federal Institute of Parana (IFPR)
Avenue: Av. José Felipe Tequinha, 1400 – Jardim das Nações
City: Paranavai
Country: Brazil
Email: gilson.kanashiro@ifpr.edu.br